IEEE Access
Multidisciplinary | Rapid Review | Open Access Journal

Received June 19, 2019, accepted June 30, 2019, date of publication July 19, 2019, date of current version August 1, 2019.

Digital Object Identifier 10.1109/ACCESS.2019.2928619

Multi-Objective Configuration Optimization for Isolated Microgrid With Shiftable Loads and Mobile Energy Storage

YUANMING SONG, YAJIE LIU, RUI WANG, AND MENGJUN MING
College of Systems Engineering, National University of Defense Technology, Changsha 410073, China

Corresponding author: Yajie Liu (liuyajie@nudt.edu.cn)

This work was supported in part by the National Natural Science Foundation of China under Grant 71371181 and Grant 71571187, and in part by the Excellent Youth Foundation of the Hunan Scientific Committee under Grant 2017JJ1001.

ABSTRACT For remote structures in military applications located in high mountains and outlying islands, the configuration of isolated microgrids constructed in these locations is highly important. To denote oxygen generation/seawater desalination devices and military battery packs in practical applications, shiftable load models and mobile energy storage models are used. A multiobjective optimization model, including the annual system cost, demand shortage rate, and the ratio of diesel energy supply, is constructed for configuration design. This model is solved using the improved preference-incentive coevolution algorithm (PICEA-ng) presented in this paper. Based on practical data and numerical simulation, the utilization strategy in terms of lost time and output power for mobile energy storage, stationary energy storage, diesel generators, and shiftable loads are generated and validated. Finally, the operational performance of the shiftable load and mobile energy storage over the entire microgrid system is analyzed and discussed.

INDEX TERMS Microgrid, multiobjective optimization, mobile energy storage, shiftable load, power allocation strategy.

I. INTRODUCTION

In remote regions, e.g., military bases built on high mountains and outlying islands, isolated microgrids are one of the most useful approaches to addressing electricity supply requirements. On the one hand, because of the long distances and complex geographical conditions, it is difficult to transmit electricity from the main electric grid to these regions. On the other hand, as types of renewable energy, the wind and solar power in these regions are usually sufficient, providing a strong possibility to establish microgrids. The optimization of an isolated electric microgrid's configuration is very important in practice. Nevertheless, such optimization is not worthwhile until several essential characteristics are considered: 1) the continuous improvement of electric military equipment utilizing batteries must provide different types of mobile and stationary energy storage devices; 2) regarded as shiftable loads, seawater desalination and oxygen generation devices must be able to regulate the operation of the electric microgrids; and 3) optimization considering a single objective is not sufficient to access various optimization goals and directions. Therefore, based on multiobjective optimization algorithms (namely, PICEA-ng), the optimization of the configuration of isolated microgrids with shiftable loads and mobile energy storage is explored in this paper.

Intelligent algorithms for the configuration optimization of microgrids have recently become very popular. For selecting optimization objectives, the research has evolved from traditional single-objective to multiobjective optimization focused on algorithmic and structural innovation [1]–[3]. Many factors are considered and constructed using actual data to achieve more realistic models [4]. For instance, the position of the sun is considered to be an environmental condition, and the wind speed varies with respect to the height. In addition, the installation angle of the photovoltaic panel and the height of the wind turbine are further considered as decision variables [5]. Reference [6] separately studied the configurations of solar and wind energy storage systems and established a two-layer decision model based on a dynamic programming method. In [7], a comprehensive

The associate editor coordinating the review of this manuscript and approving it for publication was Zhiyi Li.

cost is targeted, and the capacity optimization problem of an off-grid complementary wind-solar microgrid system was analyzed. Reference [8] discusses the influence of different control strategies on the microgrid capacity optimization. Due to this multienergy complementarity, the reliability of a typical microgrid system consisting of photovoltaic and wind power, energy storage, and diesel generators is satisfactory; thus, such systems have been widely investigated, and numerous research results on planning a whole system [9] or individual components [10] have been reported. In References [12], [13], a composite energy storage device consisting of a supercapacitor and battery is proposed to smooth power fluctuations. Reference [14] optimized a system based mainly on wind power and storage, especially considering the pumped storage capacity. Although these studies introduced new approaches to improve and expand the framework of microgrid systems [12]–[16], there remain certain reliability and financial issues to be addressed by research on the optimization of microgrid configurations.

Because of their ability to store and discharge electricity at any time, energy storage systems are a good fit for regulating the fluctuations of microgrid electricity supplies. Recent research on the regulation capacity of mobile energy storage has focused mainly on a microgrid connected to a main grid [17], whereas off-grid system research has been limited. The relevant results have focused mainly on microgrid operation scheduling [18], energy management, and charging pile planning and operation [19], while only a small portion of the literature has considered the impact of mobile energy storage on other energy unit planning, and the energy storage characteristics have usually not been considered in the design process of the operating strategy, which results in the full use of the energy storage being impossible [20] or the optimization being conducted on capacity without operational considerations [21]. In addition, the optimization of the microgrid capacity in the above studies often selects a single economic target [19]; however, the ability to make a comprehensive trade-off is preferred for most users when making decisions, and that makes multiobjective optimization more practical. In contrast, the exploration of microgrid system regulation using shiftable loads has been comparably extensive at this stage.

Reference [22] combined a power supply with several possible combinations of other components of the microgrid to establish a comprehensive system, and the practical value of this method was illustrated with the goal of lowering desalination costs. In [23], differential evolution algorithms were used to solve a multiobjective microgrid programming model including photovoltaic panels, wind generators, energy storage, diesel generators, and seawater desalination loads. Despite researchers having made numerous advances, some improvements in absorbing residual power via a shiftable load-shedding strategy remain necessary.

Specifically considering a shiftable load and mobile energy storage that have not been used in normal microgrid planning and operation studies before, this paper targets the configuration of isolated microgrids for military applications in remote areas. Furthermore, other components of microgrids, such as wind generators, photovoltaic panels, stationary energy storage, and diesel generators, have also been considered in the configuration optimization process. A power allocation strategy is established taking the component characteristics into account, and a configuration optimization model is established with multiple objectives. Then, a simulation strategy is developed for mobile energy storage management based on the unified use and management of military battery packs, in which the satisfaction of the mission requirements for the mobile energy storage device itself is fully considered. Finally, practical data are employed for a performance illustration and validation.

Notably, the work of this article is based on a previous conference paper of mine [24]. Due to the limitations on the length of the conference article, the previous work reported only a simple experiment, describing a small part of the research. In contrast, the complete model and sufficient experiments are presented in this paper.

NOMENCLATURE [24]

ρ	Air density
f	Annual inflation rate
i	Annual real interest rate
i_{nom}	Nominal interest rate
t	Number of hours that the microgrid has been running
t_{op}	Total operating time of the microgrid in one year
η_{wg}	Performance parameter of the wind turbine
v_{wg}	Wind speed at the top of the wind turbine tower
v_{ref}	Wind speed measured at the reference height
Δt	Simulation time step (1 hour in this paper)
T	Sequence number of mission periods
M	Mobile energy storage battery capacity
G_{sft}	Hourly output of a single desalination/oxygen generator
S_{rot}	Cross-sectional area of the wind turbine rotor
L_{com}	Life of a component
$I_{sc,stc}$	Short-circuit current of the photovoltaic panel under standard test conditions (temperature: 25 °C, radiant energy: 1 kW/m^2)
$R_{sft}^{\min}$	Minimum water/oxygen reserves required to address emergencies
V_{bat}	Open-circuit voltage of a single battery
$V_{oc,stc}$	Open-circuit voltage of the photovoltaic panel under standard test conditions (temperature: 25 °C, radiant energy: 1 kW/m^2)
H_{wg}	Height of wind turbine tower
H_{ref}	Reference height
C_{inv}	Initial investment cost of a component
C_{bat}	Cost of single battery unit
C_{repair}	Cost of microgrid operation and maintenance
C_{fuel}	Cost of fuel consumed by the diesel engines
$C_{replace}$	Cost of replacing the stationary energy storage battery
V_{ci}	Cut-in wind speed

V_{rat}	Rated wind speed
V_{co}	Cut-out wind speed
N_{sft}	Total number of desalination/oxygen generator units
N_{op}^{T}	Total number of mission periods of mobile energy storage in microgrid operation in one year
N_{bat}^{M}	Number of mobile energy storage units
N_{bat}^{S}	Number of stationary energy storage units
$N_{replace}$	Number of times that the battery pack has been replaced during the life cycle of the microgrid
P_{r}^{dg}	Rated output power of the diesel engine
P_{r}^{sft}	Rated power of a single desalination/oxygen generator
P_{r}^{wg}	Rated power of the wind turbine
$P_{sbp,o}^{\max}$	Maximum discharge power of a single battery pack
$P_{sbp,i}^{\max}$	Maximum charge power of a single battery pack
$P_{dg}^{\min}$	Minimum output power of the diesel generator
$P_{dg}^{\max}$	Maximum output power of the diesel generator
γ_1, γ_2	Fuel consumption coefficients
K_i, K_v	Corresponding temperature coefficients
CAP_{bu}	Total usable capacity of the storage unit
CAP_{bu}^{M}	Total available capacity of the mobile energy storage
CAP_{bu}^{S}	Total usable capacity of the stationary energy storage
CAP_{bat}^{M}	Total capacity of the mobile energy storage devices
CAP_{bat}^{S}	Capacity of the stationary energy storage unit
POW_{dg}	Annual power generation of the diesel generators
POW_{grid}	Annual electricity generation of the whole grid
POP_{i}^{max}	Nominal maximum power input of a battery pack calculated by the parameters given by its manufacturer
POP_{o}^{max}	Nominal maximum power output of a battery pack calculated by the parameters given by its manufacturer
SOC_u	*SOC* of the storage unit based on its usable capacity
$SOC^{S,max}$	Upper limit of state of charge (*SOC*) of the stationary energy storage unit
$SOC^{S,\min}$	Lower limit of the *SOC* of the stationary energy storage unit
$NCOT$	Rated temperature given by the supplier at which the photovoltaic panel will operate normally
$t_{tas}(T)$	Duration of the mission period T
$t_{lac}(T)$	Time period when mission requirements are not met
$CAP^{M}(T)$	Total available capacity of the online mobile energy storage
$CAP_{swi}^{M}(T)$	Total available capacity of the batteries switched from the ongrid to offgrid state
$SOC^{M}(T)$	*SOC* of the online mobile energy storage
$T_a(t)$	Ambient temperature in the t^{th} hour
$F_{cons}(t)$	Fuel consumption in the t^{th} hour
$E_{avail}(t)$	Electrical energy of microgrid available to all loads on the microgrid at the end of the t^{th} hour
$E_{req}(t)$	Electrical energy required by all loads on the microgrid at the end of the t^{th} hour
$R_{sft}(t)$	Water/oxygen reserves at the end of the t^{th} hour
$R_{qu}(t)$	Water/oxygen demand in the t^{th} hour
$N_{sft}^{min}(t)$	Lower limit of desalination/oxygen generator unit that can be turned on in the t^{th} hour
$N_{sft}^{max}(t)$	Upper limit of desalination/oxygen generator unit that can be turned on in the t^{th} hour
$P_{bat,i}^{\max}(t)$	Upper limit of the charge power of the energy storage
$P_{bat,i}^{\min}(t)$	Lower limit of the charge power of the energy storage
$P_{bat,o}^{\max}(t)$	Upper limit of the discharge power of the energy storage
$P_{bat,o}^{\min}(t)$	Lower limit of the discharge power of the energy storage
$P_{bat,i}^{M}(t)$	Charge power of the mobile energy storage
$P_{bat,i}^{M,\max}(t)$	Upper limit of the charge power of the mobile energy storage in the t^{th} hour
$P_{bat,o}^{M,\max}(t)$	Upper limit of the discharge power of the mobile energy storage in the t^{th} hour
$P_{bat,o}^{M}(t)$	Mobile energy storage discharge power in the t^{th} hour
$P_{bat,i}^{S}(t)$	Charge power of the stationary energy storage in the t^{th} hour
$P_{bat,i}^{S,\max}(t)$	Upper limit of the charge power of the stationary energy storage in the t^{th} hour
$P_{bat,o}^{S,\max}(t)$	Upper limit of the discharge power of the stationary energy storage in the t^{th} hour
$P_{bat,o}^{S}(t)$	Stationary energy storage discharge power in the t^{th} hour
$P_{dg}(t)$	Actual output power of the diesel engine in the t^{th} hour
$P_{or}(t)$	Ordinary load power at the end of the t^{th} hour
$P_{s,sft}^{dif}(t)$	Difference between the upper and lower power limits of the shiftable load in the t^{th} hour
$P_{s,sft}(t)$	Total load power of the desalination/oxygen system at the t^{th} hour
$S_p(t, \beta)$	Effective component of solar radiation perpendicular to the inclined surface
$P_m(t, \beta)$	Total output power of the photovoltaic panel array

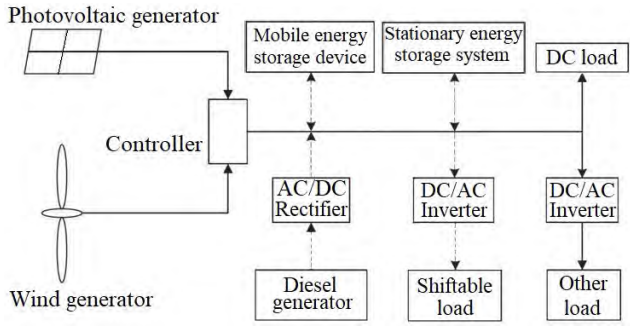

FIGURE 1. The structure of the isolated microgrid with shiftable loads and mobile energy storage.

II. COMPONENT MODELS

In this paper, the framework of the proposed isolated microgrid with a shiftable load unit and mobile energy storage device is shown in Figure 1. The main components are the photovoltaic generator, wind generator, stationary energy storage system, mobile energy storage device, diesel generator set, shiftable load, and conventional load. Before establishing the configuration optimization model of the microgrid, we must establish basic mathematical models of its primary components, in which some abstract processing and actual operational limitations of the system components should be considered. The following subsections present the detailed construction of the component models of the distributed generator, load, and energy storage.

A. ENERGY STORAGE MODEL

Because of the two types of components (stationary and mobile) in the energy storage system, CAP_{bu} is used to indicate the total usable capacity of the storage unit, and SOC_u is the SOC of the storage unit based on the usable capacity [24] ($0 \le SOC_u \le 1$). This approach is beneficial to addressing the problem that the SOC state supervision is complicated and may be overused due to the excessive number of energy storage batteries in the microgrid. The calculation approaches are given below.

1) TOTAL USABLE CAPACITY OF MOBILE ENERGY STORAGE SYSTEM

The total available capacity of the mobile energy storage system (CAP^M_{bu}) is calculated as follows [24]:

$$CAP^M_{bu} = \sum_{i=1}^{N^M_{bat}} CAP_i \cdot (SOC_i^{M,max} - SOC_i^{M,min}); \quad (1)$$

where $CAP_1 \sim CAP_{N^M_{bat}}$ is the capacity of every type of mobile energy storage device and $SOC_i^{M,max}$ and $SOC_i^{M,\min}$ are the limits of their SOC.

2) TOTAL USABLE CAPACITY OF STATIONARY ENERGY STORAGE SYSTEM

As a hypothesis, all the stationary energy storage devices are of the same specifications and have the same performance parameters. Thus, the total usable capacity of the stationary energy storage in the microgrid system (CAP^S_{bu}) is calculated by the following formula:

$$CAP^S_{bu} = N^S_{bat} CAP^S_{bat} \cdot (SOC^S_{max} - SOC^S_{\min}) \quad (2)$$

3) INPUT AND OUTPUT POWER LIMITS

When the energy storage battery is shipped from the factory, based on the battery's operating principle, materials and process, there are already certain limits of its SOC to ensure safe operation. Therefore, the maximum discharge limit and charge limit of the energy storage battery are obtained as follows:

When Discharging:

$$P^{\min}_{bat,o}(t) = 0; \quad (3)$$

$$P^{max}_{bat,o}(t) = \min\{POP^{\max}_o, SOC_u(t) \cdot V_{bat} \cdot CAP^S_{bu}/\Delta t\}; \quad (4)$$

When Charging:

$$P^{\min}_{bat,i}(t) = 0; \quad (5)$$

$$P^{\max}_{bat,i}(t) = min\{POP^{\max}_i, (1 - SOC_u(t)) \cdot V_{bat} \cdot CAP^S_{bu}/\Delta t\}; \quad (6)$$

where $SOC_u(t) \cdot V_{bat} \cdot CAP^S_{bu}/\Delta t$ is the maximum discharge power in a single simulation step (1 h) and $(1 - SOC_u(t)) \cdot V_{bat} \cdot CAP^S_{bu}/\Delta t$ is the maximum charge power in a single simulation step (1 h), and both are determined by the remaining capacity of the given battery pack. For different types of batteries, the calculation results of the input and output power limits are different due to their different parameters in the formula above.

B. MODEL OF DISTRIBUTED GENERATORS

In this paper, since the modeling techniques for distributed generators are comparatively well developed, advanced mathematical models are used for further study, e.g., a wind turbine model considering both the turbine and the tower [5]; a photovoltaic power generation system model considering the solar intensity, ambient temperature [6], position of the sun, and inclination β of the photovoltaic panel [5] and a diesel generator system model [25].

1) WIND GENERATOR

In this paper, the wind generator system is divided into two parts: the wind turbine and the wind turbine tower. The height of the wind turbine tower can fall only in a certain range and will result in cost changes for the system; this will also affect the height of the wind turbine installed at the top of the wind turbine tower. In general, wind turbines can achieve higher wind speeds at higher altitudes to drive the generator blades and generate more electrical energy under the same wind conditions.

To ensure safety, the wind turbine output is limited by the cut-in and cut-out wind speeds set by the factory. Here, an exponential law is used to convert the wind speed measured at a reference height at a particular moment into the

wind speed required at that moment in the model. As a simple model for the vertical wind speed distribution, the calculation method is [5]

$$v_{wg} = v_{ref}\left(\frac{H_{wg}}{H_{ref}}\right)^{\frac{1}{7}} \tag{7}$$

The height range of the wind turbine tower is set to $[H_{low}, H_{high}]$. When the wind speed v_{wg} corresponding to a certain height of the wind turbine tower is obtained, the wind turbine output can be calculated by the formula:

$$P_{wg}(v_{wg}) \begin{cases} 0, & if\ v_{wg} < V_{ci}; \\ \frac{1}{2}S_{rot}\eta_{wg}\rho v_{wg}^3, & if\ V_{ci} \le v_{wg} \le V_{rat}; \\ P_r^{wg}, & if\ V_{rat} \le v_{wg} \le V_{co}; \\ 0, & if\ v_{wg} \ge V_{co}; \end{cases} \tag{8}$$

where the performance parameter η_{wg} is defined as the ratio of the actual power output to the maximum power output.

2) PHOTOVOLTAIC POWER GENERATION SYSTEM

Photovoltaic panels have always suffered from a low power production per unit area; if advanced follow-up methods are applied, the vertical incidence of the sunlight can always be ensured, thereby increasing the power generation per unit area compared to that of fixed-type photovoltaic panels. However, at this stage, although the plane of the photovoltaic panel can always be completely pointed normal to the sun, the relatively complicated follow-up structure adds additional maintenance costs and reduces the reliability of the photovoltaic power generation system. Therefore, although fixed photovoltaic panels have certain disadvantages, they still represent the mainstream of the photovoltaic power plants in operation. In this paper, the optimization of the installation angle of the photovoltaic panels is still considered. Here, using the method proposed in [5], the position of the sun and the inclination of the photovoltaic panel are further considered based on the light intensity and the ambient temperature.

First, we calculate the photovoltaic panel temperature at time t,

$$T_c(t) = T_a(t) + \frac{NCOT - 20}{800}S_p(t, \beta); \tag{9}$$

where S_p is the effective component of the solar radiation perpendicular to the inclined surface; the method for calculating S_p is described in [5].

The short-circuit current I_{sc} and open-circuit voltage V_{oc} of the photovoltaic element at time t are calculated as follows:

$$I_{sc}(t) = [I_{sc,stc} + K_i(T_c(t) - 25)]\frac{S_p(t, \beta)}{1000} \tag{10}$$

$$V_{oc}(t) = V_{oc,stc} - K_v \cdot T_c(t) \tag{11}$$

The maximum output power of the photovoltaic panel considering the ambient temperature effect at time t can be determined by the formula [28]

$$P_m(t, \beta) = N_s \cdot N_p \cdot V_{oc}(t) \cdot I_{sc}(t, \beta) \cdot FF(t); \tag{12}$$

where $P_m(t, \beta)$ is the total output power of the photovoltaic panel array, which consists of N_s photovoltaic panels in series and N_p photovoltaic panels in parallel, and the fill factor $FF(t)$ is equal to the maximum power output of the photovoltaic cell divided by the product of the open-circuit voltage and the short-circuit current of the photovoltaic panel.

3) DIESEL GENERATOR

Diesel engines are typically used in microgrid systems to fill in the renewable energy output valleys and smooth the energy supply. The fuel consumption of the diesel generator during the t^{th} hour can be calculated by the formula [29]

$$F_{cons}(t) = \gamma_1 \cdot P_r^{dg} \cdot \Delta t + \gamma_2 \cdot P_{dg}(t) \cdot \Delta t \tag{13}$$

where γ_1 is 0.08145 l/kWh and γ_2 is 0.246 l/kWh. Accessory devices in the system, such as rectifiers, inverters and control switches, have little impact on the system economy and reliability due to their low cost and simple nature; thus, this paper simplifies these components.

Diesel generators are similar to traditional coal-fired generators in terms of their consumption characteristics, subject to the above function model. From practical engineering, diesel generators have a high fuel consumption per kilowatt at low power outputs. Therefore, to ensure satisfactory efficiency, the minimum output power P_{dg}^{min} and maximum output power P_{dg}^{max} of the diesel generator are limited.

C. MICROGRID LOAD

1) SHIFTABLE LOAD

In this paper, because the studied isolated microgrid is used mainly on high mountains and remote islands, we consider mainly two types of shiftable loads: a seawater desalination system and a plateau oxygen generation system. Since the functions of these two types of components resemble each other from the overall system perspective, they are abstracted by identical models [23]. Composed of multiple desalination/oxygen generators and reservoirs/storage tanks, the shiftable load system can be switched on and off based on load conditions as well as the power output of the power sources in the microgrid at a given time. The total power requirement of the shiftable load system at the t^{th} hour ($P_{s,sft}(t)$) satisfies $0 \le P_{s,sft}(t) \le N_{sft}P_r^{sft}$ [24].

2) OTHER LOADS

Other than the shiftable loads, the remaining loads consist mainly of residential electricity consumption on the microgrid.

III. MICROGRID PLANNING AND DESIGN MODEL

A. OPTIMIZATION OBJECTIVES

To be economically profitable, ensure a stable and reliable power supply, and minimize the abandonment of solar power and wind power, the diesel energy supply rate (*DER*), the annual cost of the system (*ACS*), and the ratio of demand lack (*RDL*) are determined as the optimization targets in this

paper and can be expressed as [24]

$$MinF_{obj} = (DER, ACS, RDL) \tag{14}$$

where F_{obj} is a function of these three targets. The detailed formulations of these three optimization goals are as follows.

1) ANNUALIZED COST OF SYSTEM

Acquired by converting expenses across the whole lifecycle to a cost per year according to the assumed life of the system, the annualized cost of the system (ACS) is calculated based on the annual interest ratio, inflation rate, and other parameters and can effectively reveal the annual financial benefits of the microgrid system. The calculation of ACS is as follows:

$$ACS = C_{initial} + C_{replace} + C_{repair} + C_{fuel} \tag{15}$$

In equation (15), $C_{initial}$ refers to the initial investment cost of the system [5], which includes the purchase, transportation, and installation expenditures of the microgrid devices, in addition to the shiftable load and mobile energy storage; $C_{repair}(k)$ is the operation and maintenance costs in the k^{th} year. The cost of the energy storage components includes only the costs of the stationary energy storage system and the cost of necessary facilities for accessing the mobile energy storage devices; the initial investment, component replacement and operation and maintenance costs of the mobile energy storage system are not included. In calculating the annualized cost of the microgrid, the nominal interest rate and the annual inflation rate are taken as 3.75% and 1.5%, respectively. The calculation method of each item in equation (15) is as follows:

$$\begin{aligned} C_{initial} &= \sum C_{cinv} \cdot \frac{i \cdot (1+i)^{L_{com}}}{(1+i)^{L_{com}} - 1}, \quad i = \frac{i_{nom} - f}{1+f}; \\ C_{replace} &= C_{bat} \cdot N_{bat}^{S} \cdot N_{replace}; \\ C_{repair}(k) &= C_{repair}(1) \cdot (1+f)^{k}; \\ C_{fuel} &= \sum_{t=1}^{t_{op}} F_{cons}(t). \end{aligned} \tag{16}$$

2) RATIO OF DEMAND LACK

The RDL is defined as the proportion of time during microgrid operation during which the electricity supply is not able to meet the demands of the mobile energy storage system or loads. The calculation method is as follows:

$$RDL = \frac{\sum_{t=1}^{t_{op}} Bl\,(t) + \sum_{T=1}^{N_{op}^{T}} t_{lac}\,(T)}{2t_{op}} \tag{17}$$

The formula used to calculate $t_{lac}\,(T)$ is described in Section III-B. As a Boolean value, $Bl\,(t)$ is calculated by equation (18) [25]:

$$Bl\,(t) = \begin{cases} 0, & if\ E_{avail}\,(t) > E_{req}\,(t)\,; \\ 1, & if\ E_{avail}\,(t) < E_{req}\,(t)\,. \end{cases} \tag{18}$$

The value of RDL is between 0 and 1, where 0 means that the load demand can always be satisfied during the cycle. Here, the time-series method is used to calculate the missing demand.

3) RATIO OF DIESEL ENERGY

This goal, illustrated by equation (19), is to minimize the consumption of nonrenewable energy during the full lifecycle of the designed microgrid; this goal is equivalent to maximizing the proportion of renewable energy in the system's energy supply.

$$DER = \frac{POW_{dg}}{POW_{grid}} \times 100\% \tag{19}$$

B. TASK SIMULATION OF MOBILE ENERGY STORAGE COMPONENT

Being defined by the specified operational simulation, the mobile energy storage system has its own mission requirements in this paper; here, the power-absorbing ability of the system is limited.

The 24-hour operating time of the mobile energy storage devices, whose total capacity is CAP_{bat}^{M}, is divided into 3 parts: the interval of 07:00-13:00 is mission period 1 (6 h); the interval of 13:00-19:00 is mission period 2 (6 h), and the interval of 19:00-07:00 (the next day) is mission period 3 (12 h). During each mission period, the discharge/charge state is invariant. For example, the state of being offline or online is switched at the transition point of each time interval based on the task schedule.

Switching occurs at 07:00 (transition point 1), 13:00 (transition point 2) and 19:00 (transition point 3) based on the definitions of the mission periods. The ongrid and offgrid probabilities at each conversion point of the mobile energy storage devices vary based on the characteristics of the subsequent mission period. When conducting this transition, the state of each battery is initially monitored. Then, all the battery capacities are summed to obtain the overall capacity and total SOC [24]. In this paper, the simulation step size is 1 hour. Hence, $T+1$ in equations (20) and (21) indicate the transition to the next mission period. The initial SOC is 100%.

The conversion rules for transition point 1 are given in Table 1.

The calculation method for the total available capacity of the ongrid mobile energy storage devices in Table 1 is as follows:

$$CAP^{M}\,(T+1) = CAP^{M}\,(T) + n_1 \cdot CAP_{bat}^{M} - m_1 \cdot CAP_{bat}^{M}; \tag{20}$$

where CAP^{M} in the next mission period is obtained by adding the total capacities of the batteries that switch to the online state in the current mission period to CAP^{M} in the last mission period and subtracting the capacity of the newly offline batteries. The meanings of n_1 and m_1 are shown in Table 1.

TABLE 1. Conversion rules.

Conversion point 1				
State				State of charge (single battery residual ratio)
Before conversion	Conversion probability	After conversion	Number of converted batteries	
offline$^a_{sin}$	100%	online	n_1	20%
online	50%	offline$^a_{sin}$	m_1	100%
	50%	online	$M - n_1 - m_1$	100%

^{a}offline^{sin} means the state of the battery at which the battery packs remain offline for only one mission period.

The SOC is

$$SOC^M(T+1) = SOC^M(T) + 0.2n_1 \cdot CAP^M_{bat} - m_1 \cdot CAP^M_{bat}; \quad (21)$$

where SOC^M in the next mission period is calculated by adding the residual energy of the batteries that switch to the online state in the current mission period to the SOC^M in the last mission period and subtracting the residual energy of the newly offline batteries.

The conversion rules of transition points 2 and 3 (see Table 6) resemble those of transition point 1, except for the switching probability between every state. In the simulation, the offgrid mobile storage units have a 50% probability of switching to the ongrid state at transition point 2, while the remaining units continue executing their tasks. The ongrid mobile storage units have a 50% probability of being switched to the offgrid state, and the remaining units remain in the ongrid state. At conversion point 3, the offgrid units are all switched to the ongrid state, where the ongrid devices switch to the offgrid state with a 20% probability.

The transition rules above regard all mobile energy storage devices as a whole system, the SOC and capacity of which change randomly according to the attribute values of each battery at the conversion time. In addition, $SOC^M(T)$ may take on a negative value. Thus, when $SOC^M(T) < 0$, it is included in the calculation of the RDL. The lack time of the mission demand $t_{lac}(T)$ (hour) is given by

$$t_{lac}(T) = \frac{\left|SOC^M(T)\right|}{CAP^M_{swi}(T)} \times t_{tas}(T); \quad (22)$$

where $CAP^M_{swi}(T)$ is the total available capacity of the batteries that switched from the ongrid to offgrid state at the time at which $SOC^M(T) < 0$.

C. OPERATIONAL STRATEGIES CONSIDERING LOAD POWER REGULATION AND MOBILE ENERGY STORAGE CHARACTERISTICS

1) POWER REGULATION LIMITS OF SHIFTABLE LOAD

At each moment, the upper and lower power limits of the shiftable load in the power control process of the microgrid system should be determined first; these limits reflect the adjustment ability of these loads at a given time. Here, the upper and lower power limits of the shiftable load in each hour are obtained based on the oxygen storage tank or reservoir capacities, the amount of oxygen or desalinated seawater being generated and the oxygen or water demands of the residents.

a: CALCULATION OF LOWER POWER LIMIT

For a given time, the upper and lower power limits of the oxygen generation/seawater desalination devices are calculated based on the demands by residents and the current water storage/oxygen reserves. The calculation of the lower power limit of the shiftable load ($P^{\min}_{s,sft}(t)$) at the t^{th} hour is as follows:

$$P^{\min}_{s,sft}(t) = N^{min}_{sft}(t) \cdot P^{sft}_r \quad (23)$$

When $R_{sft}(t-1) - R^{\min}_{sft} \geq R_{qu}(t)$, the oxygen/water storage level is sufficient. Under this condition, all the shiftable loads can be cut off from the microgrid system, which means that $N^{min}_{sft} = 0$. When $R_{sft}(t-1) - R^{\min}_{sft} < R_{qu}(t)$, the oxygen/water storage level is not sufficient. Hence, the minimum amount of oxygen generation/seawater desalination generation to be started should be calculated based on the difference between the oxygen/water storage levels at this time and the minimum water/oxygen reserve levels for ensuring the coverage of the residents' emergency demands. Hence, we have

$$N^{min}_{sft}(t) = \lceil R_{qu}(t) - \left(R_{sft}(t-1) - R^{\min}_{sft}\right) \Big/ G_{sft} \rceil \quad (24)$$

Because the water/oxygen emergency reserves must be ensured, the minimum number of devices that need to be turned on should be rounded up.

The calculation of the lower power limit is also involved in the power allocation strategy of Reference [23]. In that study, the oxygen/water storage being sufficient or not at time t depended on whether the difference between the oxygen/water reserve and the maximum capacity of the oxygen/water storage tank could satisfy the water/oxygen demand at the t^{th} hour.

In the calculation method of this paper, the maximum capacity of the oxygen/water storage tank in the determination method above is changed to the minimum oxygen/water storage capacity ($R^{\min}_{sft}$) for the emergency demand; therefore,

the lower power limit of the shiftable devices can be reduced as much as possible in the condition that the emergency reserve and daily demands for oxygen/water are guaranteed. Because of its ability to increase the power control range, this method is beneficial to the power regulation of the microgrid.

b: CALCULATION OF THE UPPER POWER LIMIT

The upper power limit of shiftable devices is identified by taking the residents' oxygen/water demands, the total capacity of the reservoirs/tanks, and the current oxygen/water reserve into the calculation.

$$P_{s,sft}^{\max}(t) = N_{sft}^{\max}(t) \cdot P_r^{sft} \tag{25}$$

When $R_{sft}(t-1) + N_{sft}G_{sft} - R_{qu}(t) \leq R_{sft}^{\max}$, the oxygen/water reserve is relatively low, which means that even if all the devices are operating, reaching the maximum total capacity of the reservoirs/tanks in one hour is impossible. In this situation, $N_{sft}^{\max}(t) = N_{sft}$.

When $R_{sft}(t-1) + N_{sft}G_{sft} - R_{qu}(t) > R_{sft}^{\max}$, the oxygen/water reserve is sufficient. When all the shiftable devices are started to satisfy the oxygen/water demand, the upper capacity limit of the tank/reservoir is reached within 1 hour. Under this condition, devices need to be started as required, namely, $N_{sft}^{\max}(t) = \lceil R_{sft}^{\max} + R_{qu}(t) - R_{sft}(t-1) \big/ G_{sft} \rceil$. To clarify the peak-smoothing effect of the shiftable load units on the renewable energy power output, the number of devices that should be started is rounded up to the next integer. Moreover, the water/oxygen storage exceeding the upper limit of the total capacity is discarded.

2) MICROGRID SYSTEM OPERATION STRATEGY

In a hybrid energy system, all the components are linked by an energy flow; thus, their system model can be described using the power consumption of each component [26]. In this paper, the power consumption of the shiftable load, the power of the energy storage module, and the electric power generated by the diesel generator in the microgrid are all adjustable. In addition, because of the nature of the mobile energy storage devices, in this paper, this type of component has a priority of charging first and then discharging to achieve low charge-discharge switching times and a high charge state.

When the microgrid system is operational, renewable energy sources should be preferentially utilized to satisfy the loads. Therefore, the net power of the microgrid, $P_{net}(t)$, is introduced here to denote the power difference between the renewable energy output and the user loads at the t^{th} hour.

$$P_{net}(t) = P_{wg}(t) + P_{pv}(t) - P_{or}(t) - P_{s,sft}^{\min}(t) \tag{26}$$

The net power situation can be divided into the following three categories:

(1) $P_{net}(t) = 0$. The renewable energy output is able to satisfy all the grid loads, which means that the energy storage units in the microgrid are not used under this condition. The oxygen/water storage at a certain time is determined by the oxygen/water consumption of the residents and the productivity of the shiftable load devices.

(2) $P_{net}(t) > 0$. In this scenario, the generated electricity is greater than the electricity demand by the residents. Here, the residual power is preferentially absorbed by the energy storage devices and shiftable units in the microgrid system.

Compare $P_{net}(t)$ with $P_{s,sft}^{dif}(t)$, where $P_{s,sft}^{dif}(t)$ is defined as

$$P_{s,sft}^{dif}(t) = P_{s,sft}^{\max}(t) - P_{s,sft}^{\min}(t) \tag{27}$$

(i) When $P_{s,sft}^{dif}(t) > P_{net}(t) > 0$, the number of shiftable units that need to be started is

$$n_1 = \lfloor P_{net}(t) \big/ P_{sft} \rfloor + N_{sft}^{min}(t) \tag{28}$$

In this circumstance, $P_{s,sft}(t) = n_1 \cdot P_r^{sft}$.

(ii) When $P_{s,sft}^{dif}(t) \leq P_{net}(t) \leq P_{bat,i}^{M,\max}(t) + P_{s,sft}^{dif}(t)$, i.e., $\left(P_{net}(t) - P_{s,sft}^{dif}(t)\right) \leq P_{bat,i}^{M,\max}(t)$, the shiftable units operate at the upper power limit: $P_{s,sft}(t) = P_{s,sft}^{\max}(t)$. Therefore, the mobile energy storage system should be charged first at this time using the remaining power. Hence, we have

$$P_{bat,i}^{M}(t) = P_{net}(t) - P_{s,sft}^{dif}(t) \tag{29}$$

(iii) Finally, when $P_{net}(t) > P_{bat,i}^{M,\max}(t) + P_{s,sft}^{dif}(t)$, i.e., $\left(P_{net}(t) - P_{s,sft}^{dif}(t)\right) > P_{bat,i}^{M,\max}(t)$, the mobile energy storage system reaches the upper power absorption limit; however, electric power remains in the microgrid. Therefore, the stationary energy storage devices need to absorb the remaining electrical energy at this time.

$$P_{bat,i}^{F}(t) = P_{net}(t) - P_{s,sft}^{dif}(t) - P_{bat,i}^{M,\max}(t) \tag{30}$$

If power remains when the stationary energy storage system reaches its power-absorbing upper limit, this part of the power output is discarded. In this circumstance, $P_{bat,i}^{F}(t) = P_{bat,i}^{F,\max}(t)$.

(3) $P_{net}(t) < 0$. The power generation of the renewable energy devices cannot satisfy the full load demand when the shiftable units operate at their lower electric power limit. In this situation, the stationary energy storage devices discharge first to overcome the shortage of electricity in the microgrid.

(i) If $P_{bat,o}^{F,\max}(t) > P_{dg}^{\min} > |P_{net}(t)|$, the electric energy deficit is filled completely by the discharging power of the stationary energy storage devices: $P_{bat,o}^{F}(t) = |P_{net}(t)|$. Considering the desire to minimize the losses in their operational lifetimes, the mobile energy storage devices do not discharge under this condition.

(ii) If $P_{dg}^{\max} \geq |P_{net}(t)| \geq P_{dg}^{\min}$, the stationary energy storage devices stops discharging; simultaneously, the diesel generators are turned on. In this circumstance, $P_{dg}(t) = |P_{net}(t)|$.

(iii) When $\left(P_{bat,o}^{F,\max}(t) + P_{dg}^{\max}\right) \geq |P_{net}(t)| > P_{dg}^{\max}$, the stationary energy storage devices discharge and the diesel generators provide their full-power output, together

compensating for the electricity shortage in the microgrid. Therefore,

$$P_{dg}(t) = P_{dg}^{\max} \tag{31}$$

$$P_{bat,o}^{F}(t) = |P_{net}(t)| - P_{dg}^{\max} \tag{32}$$

(iv) When $\left(P_{bat,o}^{F,\max}(t) + P_{dg}^{\max} + P_{bat,o}^{M,\max}(t)\right) \geq |P_{net}(t)| > \left(P_{bat,o}^{F,\max}(t) + P_{dg}^{\max}\right)$, even if the stationary energy storage devices and diesel generators provide their full-power output together, the load requirements at this time still cannot be satisfied. In this situation, the mobile energy storage devices need to discharge to compensate the electric power shortage in the microgrid. Therefore,

$$P_{dg}(t) = P_{dg}^{\max} \tag{33}$$

$$P_{bat,o}^{M}(t) = |P_{net}(t)| - P_{dg}^{\max} - P_{bat,o}^{F,\max}(t) \tag{34}$$

(v) When $|P_{net}(t)| \geq \left(P_{bat,o}^{F,\max}(t) + P_{dg}^{\max} + P_{bat,o}^{M,\max}(t)\right)$, this circumstance is considered in the *RDL* calculation as a period of insufficient power supply.

IV. SOLUTION METHODOLOGY

The solution of the optimization model proposed in this paper is obtained by solving a nonlinear multiobjective problem with multiple decision variables, including the number of photovoltaic panels (N_{pv}), the installation angle of the photovoltaic panels (β), the number of wind generators (N_{wg}), the installation height of the wind generators (H_{wg}), the number of stationary energy storage components (N_{bat}^{S}), the number of diesel generators (N_{dg}), and the number of oxygen/water storage tanks (N_{wst}).

The improved preference-inspired coevolution algorithm (PICEA-ng) [27], which achieves excellent performance in solving this type of problem, is used as the solution algorithm. By introducing a set of preferences and coevolving with the candidate solution population to simultaneously provide multiple hypothetical preference sets, the algorithm searches for and obtains a better representative of the entire Pareto front. In this algorithm, the coevolutionary preference is called the target vector. However, these preferences are not the true preferences of the decision makers but rather represent a method for comparing the advantages and disadvantages of the different solutions for posterior optimization [5]. The algorithm has a strong search ability and excellent performance in solving high-dimensional (three or more) problems. The performance of the improved PICEA-g on the WFG test problem set has been proven to exceed that of four advanced multiobjective evolutionary algorithms: NSGA-II, MOEA, Hype, and MOEA/D [30]. The fitness allocation method as well as the performance of the improved algorithm based on this method (PICEA-ng) have been further improved [27].

The algorithm flowchart is shown in Figure 2.

In the solution process, the maximum iteration number is 100, and the population of the target vectors and the number of individuals in the population of the decision variables are set to 50. This algorithm uses polynomial mutation (PM) genetic operators and simulated binary crossover (SBX), along with the recombination probability P_m and crossover probability P_c. The distribution index is shown in Table 2, where n_{var} is the number of decision variables [24].

Real code technology is employed for chromosome coding because the genetic operator includes *SBX* and *PM*. Therefore, the chromosome consists of $[N_{pv}|N_{wg}|N_{bat}^{S}|N_{dg}|N_{wst}|\ \beta|\ H_{wg}]$, which contains seven decision variables. Thus, the chromosome has a 1/7 mutation probability in the polynomial mutation. Considering its practical application, the first five variables are rounded in the calculation.

During the solution process, the numbers of photovoltaic panels, wind generators, and diesel generators should be restricted within an appropriate range of values to reduce the search space of the algorithm according to the given load power demand scenario or the constraints of the occupied area. The *SOC* of each energy storage component varies within a specified range.

V. NUMERICAL EXPERIMENTS

A. EXPERIMENTAL DATA

Based on the average meteorological data [5] in a specified area from the past several decades, the annual horizontal solar radiation, hourly average wind speed measured at an altitude of 10 m, and average ambient temperature per hour are generated for the case study. In this paper, water consumption data from Reference [23] are used for the system capacity planning and calculation. The seawater desalination system has eight independent seawater desalination devices, whose rated power is 250 W, and the water production of each device is 1 t/d. The distributions of the solar radiation, wind speed and temperature utilized in this case study are shown in Figure 3 - Figure 5, respectively, and the load and water demands are illustrated in Figs. 6 (a) and (b). In the following calculation examples, for the parameters of the wind turbines, stationary energy storage units, photovoltaic panels and diesel generators, we adopted the settings from Reference [8].

B. ANALYSIS OF OPTIMIZATION RESULTS

In Figure. 7, the last generation of the results is shown as the resulting Pareto front.

In Figure 7, there is a significant negative correlation between the three objectives. From the ACS-RDL subgraph and the ACS-DER subgraph of the 3D Pareto frontier, it is obvious that reducing the demand miss rate will result in an obvious increase in the annual system cost. A reduction in the proportion of diesel generators in the total energy supply will also lead to cost increases. Specifically, to make the microgrid system more capable of satisfying the energy demands and lower the dependence on diesel generators, an increase in costs is inevitable. Therefore, the optimal solution is not unique, and it is better to comprehensively consider various factors and fully exploit the information contained in the Pareto frontier to facilitate scientific decision making.

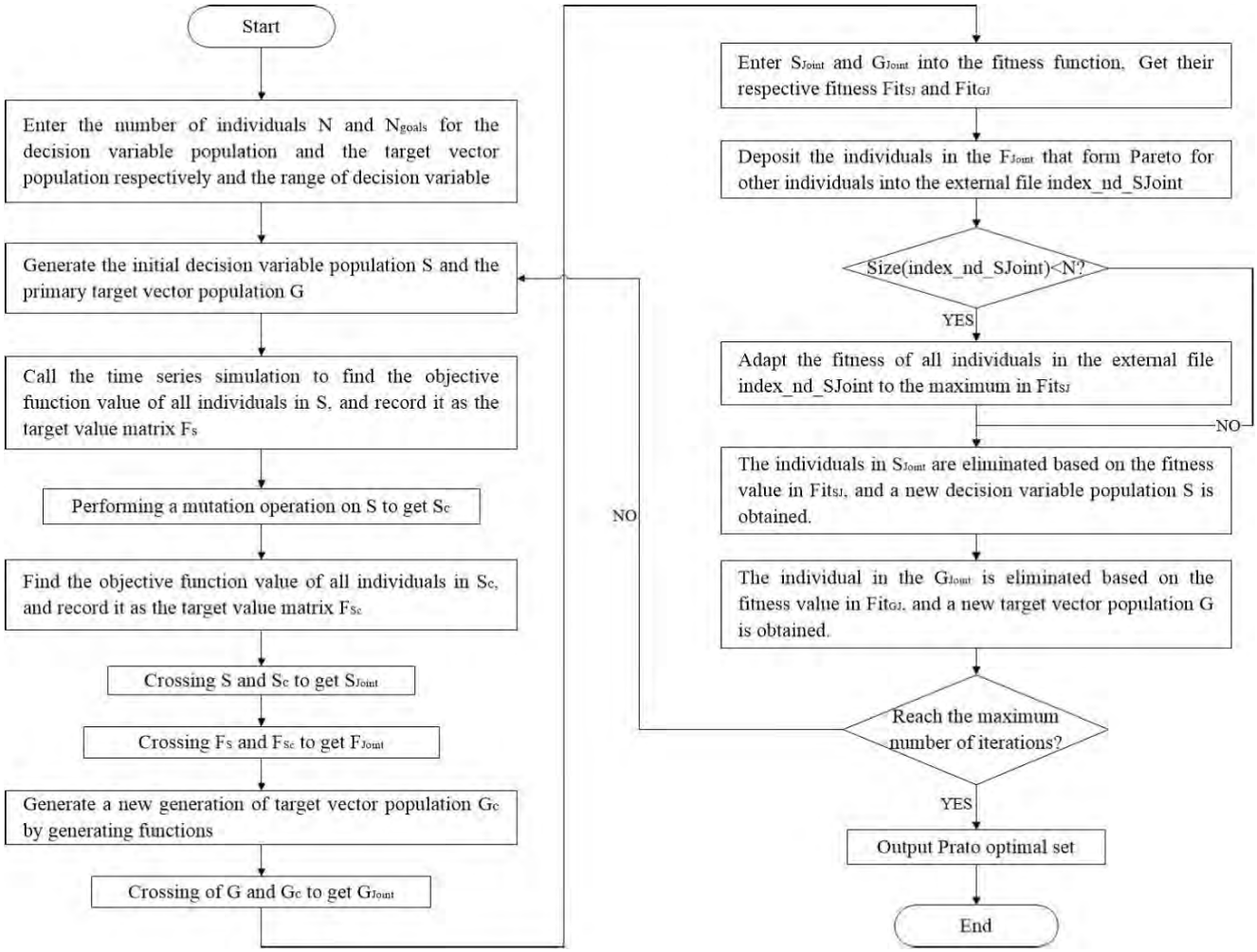

FIGURE 2. Algorithm flowchart of PICEA-ng.

TABLE 2. Algorithm parameters.

$P_c(SBX)$	$\eta_c(SBX)$	$P_m(PM)$	$\eta_m(PM)$
1	15	$1/n_{var}$	20

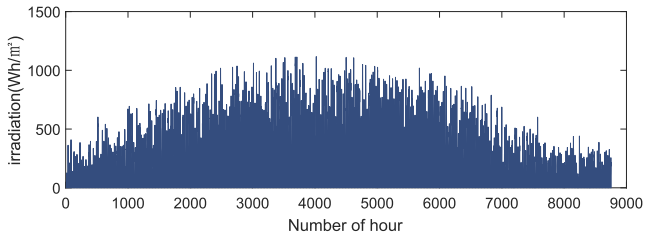

FIGURE 3. Solar radiation distribution.

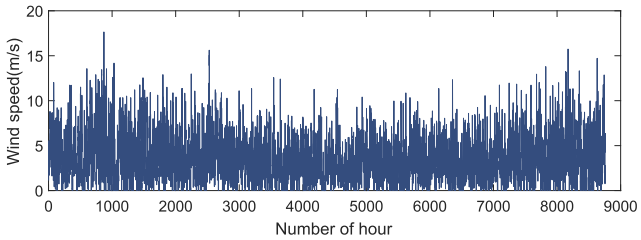

FIGURE 4. Wind speed distribution.

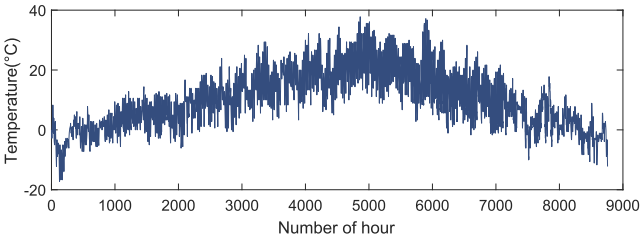

FIGURE 5. Temperature distribution.

The 50 nondominated candidate solutions obtained after 100 iterations are of the same quality. The decision makers only need to select the most satisfactory solution based on their posterior preference information. Because of the military requirements of the microgrid system, the objective *DER* is set to less than 20%. When the objective *RDL* is less than 0.1%, 0.5%, and 1%, a corresponding solution is selected from the 3D Pareto front [24]. The three consequently obtained capacity configurations are shown in Table 3.

TABLE 3. Selected capacity configuration.

	$DER(\%)$	$RDL(\%)$	$ACS(\$)$	$N_{PV}(set)$	$N_{wg}(set)$	$N_{bat}^{S}(set)$	$N_{dg}(set)$	$N_{wst}(set)$	$\beta(^\circ)$	$H_{wg}(m)$
1	15.8228	0	23233.5269	33	22	38	1	18	52.069	24.763
2	16.3646	0.3546	16180.7973	37	8	39	1	13	26.230	29.202
3	0	0.9283	23473.1673	39	22	38	0	18	10.819	29.972

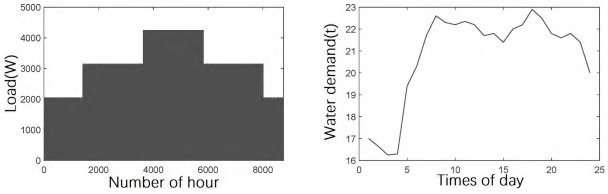

(a) Load data distribution (b) Water demand distribution

FIGURE 6. Load and water data distributions.

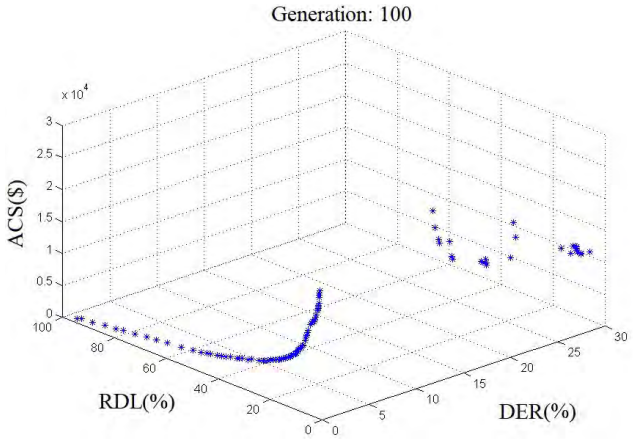

FIGURE 7. Final optimization results shown in the three-dimensional coordinate system.

When the DER or RDL is reduced to 0%, that is, when the microgrid system is completely powered by renewable energy or fully satisfies the loads, a large increase in the annualized cost (ACS) will occur, consistent with the conclusions drawn from the overall trend of the curve shown in Figure 7.

C. MODEL VALIDITY VERIFICATION

Five one-year (8760 hours) time-series simulations were performed with the capacity configuration of result 2 in Table 3. To compare with the original results, the target values of each simulation are listed in Table 4.

The comparison in Table 4 shows that the nonrenewable energy supply ratio is very stable and shows almost no fluctuations. However, there are certain changes in the demand shortage rate and the annualized cost, and the fluctuation of the demand deficiency rate is relatively large. This is because the demand shortage rate includes both the power supply demand and the mission demand for mobile energy storage. The demand for mobile energy storage tasks presents a certain randomness, which leads to fluctuations in the demand-missing rate. This randomness also causes differences in the start-stop behavior of the diesel engines in each simulation, which causes changes in the fuel consumption and consequently small fluctuations in the annualized costs. Therefore, the simulation results in the table are reasonable.

TABLE 4. Simulation results.

	$DER(\%)$	$RDL(\%)$	$ACS(\$)$
original value[a]	16.3646	0.3546	16180.7973
value[a] of 1^{st} simulation	16.3646	0.3321	16178.0295
value[a] of 2^{nd} simulation	16.3646	0.3656	16181.1437
value[a] of 3^{rd} simulation	16.3646	0.3367	16179.3574
value[a] of 4^{th} simulation	16.3646	0.3378	16178.8556
value[a] of 5^{th} simulation	16.3646	0.3743	16182.3214

[a] value refers to objective value, including DER, RDL and ACS.

Next, we observe the operational behaviors of each component in the first simulation. In the design of the simulation program, the system must satisfy all constraints during operation. Comparing Figure9(a)(b) with Figure3 and Figure4, it can be seen that the outputs of the photovoltaic generators and wind turbines depend on the actual solar intensity and wind speed data, and there is a clear positive correlation, which is in line with expectations.

Figure9(c) reflects the operating conditions of the stationary energy storage after one year from the perspective of the *SOC*. Because the stationary energy storage in the system should play the role of peak clipping and valley filling in the renewable energy output, the *SOC* of the stationary energy storage is always changing within one year. Simultaneously, during the period from 3700 hours to 4700 hours of this year, the stationary storage energy discharge depth is obviously increased, which is due to the peak power consumption in the summer, meaning that the power demands of the loads increase. When the output of the wind generators and photovoltaic panels cannot satisfy the requirements of the loads, the stationary energy storage will supply power to the loads first.

Figure9(d) shows that the output of the diesel generators varies over the course of the year, and the output during the middle of the year is relatively high. This is because the load demand increases during the middle of the year, presenting a peak in the power consumption. When the stationary energy storage is discharged but the load demand still cannot be satisfied, the starting condition of the diesel generator is reached. The diesel generator will then begin to compensate for the power shortage.

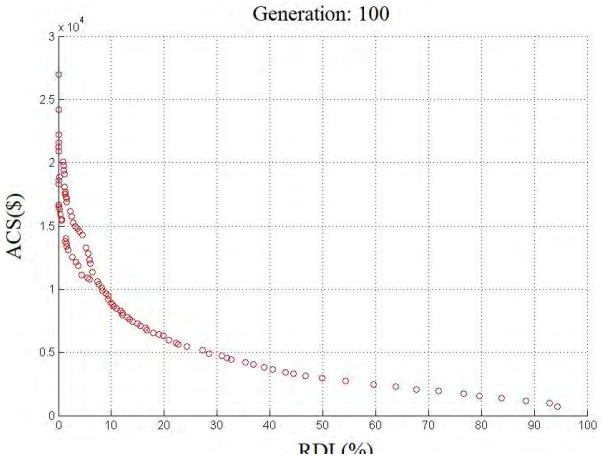

(a) ACS-RDL subgraph

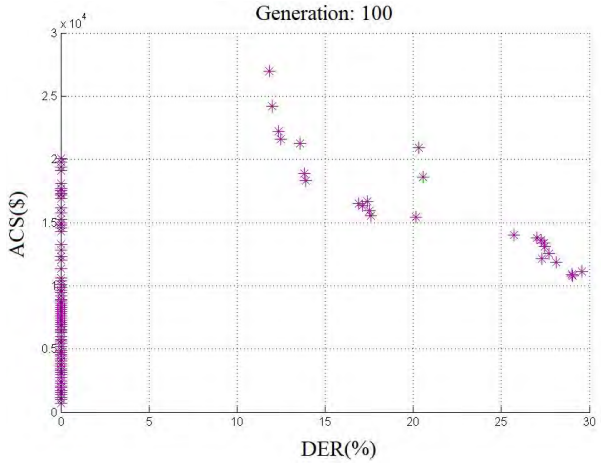

(b) ACS-DER subgraph

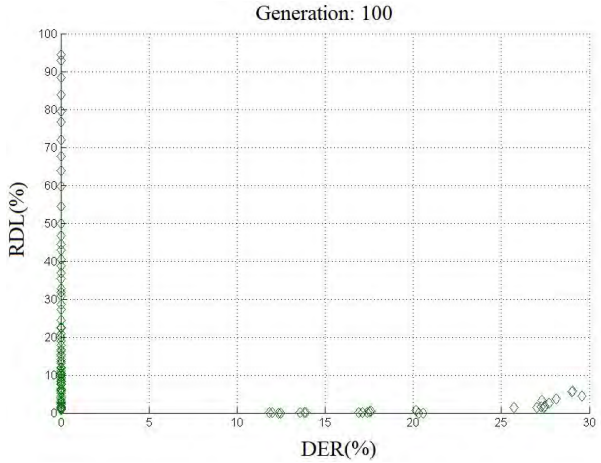

(c) RDL-DER subgraph

FIGURE 8. **Optimization results shown in the two-dimensional coordinate system.**

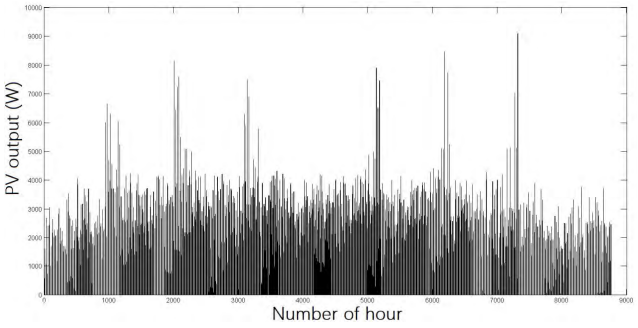

(a) Output curve of photovoltaic generator

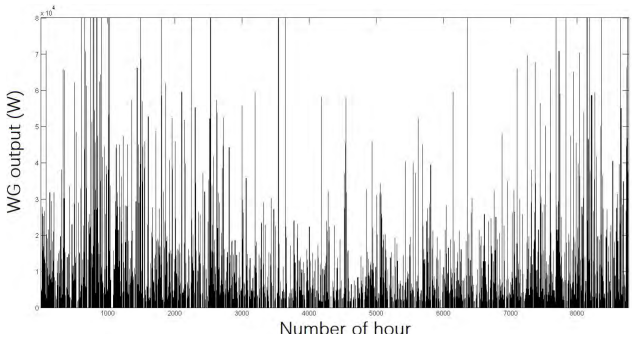

(b) Output curve of wind generator

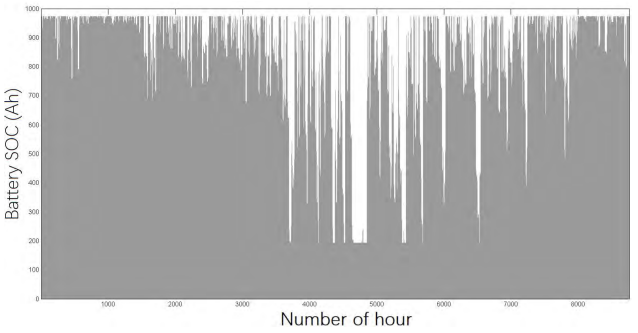

(c) SOC variation of stationary energy storage

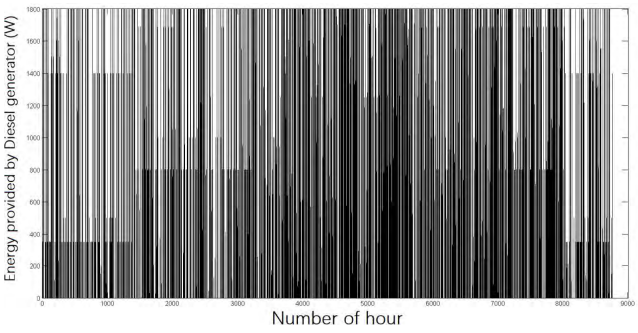

(d) Output curve of diesel generator

FIGURE 9. **Component operation condition.**

In summary, the input and output powers of each component in the model are normal, and the target value is calculated accurately, therein adequately reflecting the actual operation of the system.

D. EFFICIENCY ANALYSIS OF MOBILE ENERGY STORAGE AND SHIFTABLE LOAD

Because the shiftable units and mobile energy storage devices are introduced in the traditional microgrid structure, in addition to the observation and verification of the normal

TABLE 5. Control variable simulation results.

scheme	$RMRL(\%)$	$RLRL(\%)$	$DER(\%)$	$ACS(\$)$
1	0.2667	0.5708	16.3646	16178.0295
2	0	0.7991	16.3883	16179.4293
3	0.2942	0.6963	22.1754	16994.0402
4	0	1.0274	22.2244	16996.2541

cooperation of the components of the system (Section V-C), it is also necessary to compare and analyze the operational performance of the microgrid before and after the introduction of shiftable units and mobile energy storage devices. This is done to determine whether the shiftable units and mobile energy storage devices can function normally and whether they can achieve good power control performance in the microgrid. Here, the magnitude of the value of the optimization objectives is used to characterize the power control performance.

We take the capacity configuration shown in row 2 of Table 3 as an example [24], and multiple simulations with a length of one year (8760 hours) are performed based on the 4 types of variable control schemes shown in Table 5. Here, the optimization target values corresponding to each simulation scheme are included as well.

The data shown in Table 5 are an average of ten simulations corresponding to each scenario. The particular schemes in Table 5 are explained as follows:

Scheme 1: Maintain the original microgrid operation strategy.

Scheme 2: Mobile energy storage devices participate in the power regulation of the microgrids as ordinary loads.

Scheme 3: Shiftable units participate in the power regulation of the microgrid as ordinary loads.

Scheme 4: Shiftable units and mobile energy storage devices are both applied as ordinary loads to participate in the power regulation of the microgrid.

In this paper, RDL is one of the optimization goals, including the comprehensive statistics of the rate of the mobile energy storage devices' mission requirement loss (*RMRL*) and the rate of load requirement loss (*RLRL*). Here, *RMRL* and *RLRL* are separately listed to intuitively show the effectiveness of the mobile energy storage and shiftable loads; the calculation of *RMRL* and *RLRL* is as follows:

$$RMRL = \sum_{T=1}^{t_{op}} t_{lac}(T) \Big/ T \tag{35}$$

$$RLRL = \sum_{t=1}^{t_{op}} Bl(t) \Big/ T \tag{36}$$

The results of simulation scheme 4 are compared with the simulation results of scheme 2 and scheme 3 as follows. For scheme 2, compared with scheme 4, the load demand missing rate decreased from 1.0274% to 0.7991%. Similarly, after the mobile energy storage of scheme 3 begins participating in the microgrid power regulation, the load demand missing rate also decreased significantly (from 1.0274% to 0.6963%). Because the mobile energy storage needs to be discharged after participating in the power regulation of the microgrid, the mission demand loss rate increased from 0% to 0.2942%. The above comparison shows that the shiftable units and mobile energy storage devices have an important influence on the electric energy supply of the microgrid; however, the participation of mobile energy storage devices in the microgrid regulation has a small probability of resulting in mission failure.

TABLE 6. Supplement to conversion rules.

Conversion point 2				
State				State of charge (single battery residual ratio)
Before conversion	Conversion probability	After conversion	Number of converted batteries	
offline_{sin}	50%	online	n_2	50%
	50%	$\text{offline}^{a}_{cons}$	$m_1 - n_2$	/
online	50%	online	$M - m_1 - m_2$	/
	50%	offline_{sin}	m_2	100%

[a] offline^{cons} means the state of a battery in which the battery packs remain offline for two task periods.

Conversion point 3				
State				State of charge (single battery residual ratio)
Before conversion	Conversion probability	After conversion	Number of converted batteries	
offline_{sin}	100%	online	m_2	50%
offline_{cons}	100%	online	$m_1 - n_2$	10%
online	20%	offline_{sin}	m_3	100%
	80%	online	/	/

On the other hand, as we can see, shiftable units can reduce the annual system cost from \$16,996.2541 to \$16,179.4293 and significantly reduce the nonrenewable energy supply ratio from 22.2244% to 16.3883% [24]. The power absorbed by the shiftable units in the scenario where the wind and solar resources are sufficient is used to increase the fresh water reserves, which makes the shiftable units able to operate at lower power for the propose of reducing the diesel fuel consumption and increasing the renewable energy utilization when the power in the microgrid is insufficient. The discussion above is verified by the reduction of *ACS* and *DER*.

In contrast, if the mobile energy storage devices participate in the regulation, the discharge priority is the lowest, which means that the mobile energy storage devices are discharged after the diesel generator. Hence, the use of mobile energy storage devices cannot reduce the fuel consumption of the diesel engines; however, it is able to absorb part of the power when the wind power is sufficient and slightly increases the utilization rate of renewable energy, which is reflected in the reduction of *DER* (from 22.2244% to 22.1754%).

When the shiftable units and mobile energy storage devices participate in the regulation of the microgrid, the *RDL* decreases from 1.0274% to 0.5708%, which means that both units can play a relatively effective role together when involved in the power regulation of the microgrid system. In terms of the load demand missing rate, compared with mobile energy storage devices involved in the microgrid control, the *RLRL* is reduced from 0.2942% to 0.2667% after the shiftable load participates in the microgrid power regulation, indicating that the shiftable units and mobile energy storage devices can complement each other. Nevertheless, the predetermined starting and stopping conditions of each device related to the microgrid operation strategy still need to be further adjusted to achieve better regulation performance.

VI. CONCLUSION

For future deployments of the Chinese army, comprehensive consideration must be given to the mission requirements, living needs, and rapid development of equipment powered by electricity. Thus, renewable energy generation, controllable power supplies (diesel generators or micro gas turbines), shiftable loads (desalination loads, etc.), mobile energy storage and stationary energy storage will likely become typical components of microgrids on islands or in alpine camps. The shiftable load represented by seawater desalination and oxygen manufacturing equipment is included in the system optimization, which can smooth the electricity output of intermittent energy generators, such as wind turbines and photovoltaic generators, and improve the utilization ratio of renewable energy in the microgrid. Mobile energy storage can replace the role of fixed energy storage to a certain extent, fill the valleys of the renewable energy output, and reduce the operating cost of the system. Therefore, by incorporating traditionally independent wind power/solar power/energy storage/diesel power into microgrids and designing appropriate operational strategies, the electricity supplied by renewable and nonrenewable energy sources can complement each other, thereby increasing the renewable energy utilization and effectively reducing the system operating costs. Based on this background, this paper has conducted indepth research on a military microgrid system, including mobile energy storage devices and shiftable units.

In this paper, the structures of hybrid renewable energy microgrid systems, including mobile energy storage devices and shiftable units, and the mission requirements of mobile energy storage devices are first defined. A simulation method for mobile energy storage units based on the mission period is proposed, and the components of the system are modeled. Then, based on the synthesis and improvement of the existing strategy, an operational strategy based on the characteristics of mobile energy storage and the power regulation of loads is proposed, including the calculation method of the upper and lower power limits of the shiftable units, and the composition and connotation of the optimization objectives of the system are clarified. A military microgrid system model including mobile energy storage devices and shiftable units is then proposed. After that, the decision variable composition, optimization objective composition and model constraints are explained. The solution algorithm (PICEA-ng) for the planning model in this paper is then introduced. Finally, model solving is performed based on actual data from a remote area in Spain, the results of which are analyzed, compared and summarized.

Based on the numerical solution and analysis, the rationality of the model and power allocation strategy are verified. Three conclusions can be drawn:

1. Shiftable units and mobile energy storage devices play important regulating roles in the microgrid electric energy supply. When mobile energy storage devices participate in the system power regulation alone, their mission requirements cannot be satisfied with small probability. When shiftable units participate in microgrid adjustment, the annualized cost of the system can be reduced, and the utilization rate of the renewable energy can be obviously improved. In contrast, mobile energy storage devices participating in the system adjustment can only slightly increase the rate of renewable energy utilization.

2. Shiftable units and mobile energy storage devices can participate in system power regulation simultaneously; moreover, they can play a complementary adjustment role in microgrid operation and obtain improved performance. The predetermined starting and stopping conditions of each device related to the microgrid operation strategy still need to be further adjusted, though, to achieve better adjustment effects.

3. After mobile energy storage devices and shiftable units participate in system energy adjustment using the power allocation strategy presented in this paper, significant effects in maintaining the relative stability of the stationary energy

storage *SOC* can be achieved, as reflected in the low level of stability during the summer peak power period and the high level of stability during the non-summer peak power range [24]. These effects are conducive to reducing the number of stationary energy storage charge and discharge cycles and prolonging the devices' service lives.

Future research directions are as follows: 1. The existing results are based on the determined historical data for capacity allocation. The next step is to combine robust optimization with multiobjective evolutionary algorithms to explore new methods for uncertain planning for the microgrid.

2. We will perform a more detailed and realistic mission simulation of mobile energy storage so that its regulation of the microgrid and randomness can be more realistically reflected. We will also improve the existing model, analyze the characteristics of each component in depth, and conduct further controlled experiments based on this adjustment operation strategy to address the problem whereby the stationary energy storage may remain at the lower limit of the *SOC* during the peak hours of power consumption under the existing strategy. We will also attempt to improve the performance of the components of the microgrid system.

REFERENCES

[1] L. R. Dufo, A. J. L. Bernal, and L. J. M. Yusta, "Multi-objective optimization minimizing cost and life cycle emissions of stand-alone PV–wind–diesel systems with batteries storage," *Appl. Energy*, vol. 88, no. 11, pp. 4033–4041, 2011.

[2] Z. Youbing, B. Wei, Y. Xiaodong, R. Shuaijie, Q. Jun, and X. Luyao, "Multi-objective programming design of independent microgrid," (in Chinese), *Hangzhou, J. Zhejiang Univ. Technol.*, vol. 12, no. 6, pp. 619–623, 2016.

[3] R. Singh, R. C. Bansal, A. R. Singh, and R. Naidoo, "Multi-objective optimization of hybrid renewable energy system using reformed electric system cascade analysis for islanding and grid connected modes of operation," *IEEE Access*, vol. 6, pp. 47332–47354, 2018.

[4] N. Ming, H. Wei, and G. Jiahuan, "Research on economic operation of microgrid integration," (in Chinese), *Power Syst. Technol.*, vol. 34, no. 22, pp. 38–42, 2010.

[5] S. Zhichao, "Research on hybrid renewable energy system planning based on multi-objective evolutionary algorithm," (in Chinese), Nat. Univ. Defense Technol., Changsha, China, Tech. Rep., 2016.

[6] L. Jianlin, "Optimal allocation strategy for energy storage capacity of wind and light storage system," *Beijing, J. Elect. Eng.*, vol. 33, no. 17, pp. 1189–1196, 2018.

[7] Y. Qi, Z. Jianhua, and L. Zifa, "Multi-objective optimization design of wind-solar hybrid power supply system," (in Chinese), *Autom. Electr. Power Syst.*, vol. 33, no. 17, pp. 86–90, 2009.

[8] C. Jian, W. Chengshan, and Z. Bo, "Planning and design of independent microgrid considering different control strategies," (in Chinese), *Autom. Electr. Power Syst.*, vol. 37, no. 22, pp. 1–6, 2013.

[9] M. Xiyuan, W. Yaowen, and F. Hualiang, "Power supply planning of wind/light/storage hybrid microgrid with improved bacterial foraging algorithm," (in Chinese), *China Electr. Eng.*, vol. 31, no. 25, pp. 17–25, 2011.

[10] B. Zhao, X. Zhang, P. Li, K. Wang, J. Chen, and F. Li, "Optimal design and application of energy storage system in Dongfushan island standalone microgrid," (in Chinese), *Autom. Electr. Power Syst.*, vol. 37, no. 1, pp. 161–167, 2013.

[11] M. Mengjun, "Review of multi-objective optimization of hybrid renewable energy systems," (in Chinese), *Proc. Chin. Soc. Electr. Eng.*, vol. 38, no. 10, pp. 2908–2917, 2018.

[12] U. Akram, M. Khalid, and S. Shafiq, "An innovative hybrid wind-solar and battery-supercapacitor microgrid system—Development and optimization," *IEEE Access*, vol. 5, pp. 25897–25912, 2017.

[13] Y. Tianmeng, "Capacity optimization method for composite energy storage system in wind power system," (in Chinese), *Suzhou, Elect. Eng.*, vol. 3, no. 1, pp. 7–12, 2018.

[14] Y. Wei, "Optimization of pumped storage capacity of wind-storage combined system," (in Chinese), *Beijing, China Electr. Power.*, vol. 51, no. 2, pp. 99–105, 2018.

[15] S. Ashok, "Optimised model for community-based hybrid energy system," *Renew. Energy*, vol. 32, no. 7, pp. 1155–1164, 2007.

[16] C. Rubio-Maya, J. Uche-Marcuello, and A. Martínez-Gracia, "Design optimization of a polygeneration plant fuelled by natural gas and renewable energy sources," *Appl. Energy*, vol. 88, no. 2, pp. 449–457, 2011.

[17] W. Xinghua, "Taking into account the optimal configuration of microgrid capacity in grid-connected operation of electric vehicles," (in Chinese), *Shanghai, Electr. Autom.*, vol. 40, no. 1, pp. 36–39, 2018.

[18] M. Yuan, Y. Fu, Y. Mi, Z. Li, and C. Wang, "The coordinated control of wind-diesel hybrid micro-grid based on sliding mode method and load estimation," *IEEE Access*, vol. 6, pp. 76867–76875, 2018.

[19] A. S. Hintz, U. R. Prasanna, and K. Rajashekara, "Hybrid multi-agent based resilient control for EV connected micro grid system," in *Proc. IEEE Transp. Electrific. Conf. Expo (ITEC)*, Dearborn, MI, USA, Jun. 2014, pp. 1–6.

[20] L. Bozhen, "Microgrid planning model and algorithm considering energy storage characteristics of electric vehicles," (in Chinese), *Electr. Power Construct.*, vol. 38, no. 2, pp. 60–65, 2017.

[21] Y. Yue, "Capacity optimization of microgrid energy storage unit considering electric vehicle," (in Chinese), *Beijing, J. Instrum.*, vol. 35, no. 6, pp. 1261–1268, 2014.

[22] K. Bourouni, T. Ben M'Barek, and A. Al Taee, "Design and optimization of desalination reverse osmosis plants driven by renewable energies using genetic algorithms," *Renew. Energy*, vol. 36, no. 14, pp. 936–950, 2011.

[23] Z. Jianhua, "Capacity planning of microgrid with wind/light/cement/storage and seawater desalination load," (in Chinese), *J. Electr. Eng. Technol.*, vol. 29, no. 2, pp. 102–112, 2014.

[24] Y. Song, Y. Liu, S. Huang, T. Zhang, and R. Wang, "Multi-objective configuration optimization for isolated microgrid with mobile energy storage and shiftable load," in *Proc. 2nd IEEE Conf. Energy Internet Energy Syst. Integr. (EI2)*, Beijing, China, Oct. 2018, pp. 1–7. doi: 10.1109/EI2.2018.8582245.

[25] M. Mengjun, "Adaptive decomposition and evolution multi-objective optimization method and application," (in Chinese), Nat. Univ. Defense Technol., Changsha, China, Tech. Rep., 2017.

[26] S. Zhiyi, "Research on modeling and simulation technology of Fengguang diesel storage power generation system," (in Chinese), Beijing Jiaotong Univ., Beijing, China, Tech. Rep., 2010.

[27] Z. Shi, R. Wang, and T. Zhang, "PICEA-g using an enhanced fitness assignment method," in *Proc. IEEE Symp. Comput. Intell. Multi-Criteria Decis.-Making (MCDM)*, Dec. 2014, pp. 72–77.

[28] L. Zhenguo, "Microgrid system planning and design method based on double layer optimization," (in Chinese), *Power Syst. Protection Control*, vol. 4, no. 16, pp. 124–133, 2015.

[29] R. Dufo-López and J. L. Bernal-Agustni, "Multi-objective design of PV–wind–diesel–hydrogen–battery systems," *Renew. Energy*, vol. 33, no. 12, pp. 2559–2572, 2008.

[30] R. Wang, R. C. Purshouse, and P. J. Fleming, "Preference-inspired coevolutionary algorithms for many-objective optimization," *IEEE Trans. Evol. Comput.*, vol. 17, no. 4, pp. 474–494, Jun. 2013.

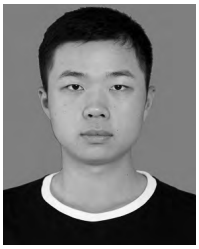

YUANMING SONG received the B.E. degree in system engineering from the National University of Defense Technology (NUDT), Changsha, China, in 2018, where he is currently pursuing the master's degree.

YAJIE LIU was born in 1975. He received the Ph.D. degree from the College of Systems Engineering, National University of Defense Technology, China, where he is currently an Associate Professor.

He was a Visiting Scholar with the Mechanical and Industrial Engineering Department, University of Toronto, from 2008 to 2009. His research interest includes planning and optimization methods for microgrids.

RUI WANG was educated in mathematics and management, and he received the Ph.D. degree in systems engineering from the University of Sheffield, U.K., in 2014, under the supervision of P. Fleming.

He is currently a Lecturer with the National University of Defense Technology (NUDT). Before he joined NUDT, he was a Visiting Researcher with IPN-Cinvestav and IIT Kanpur, in 2013, and a Research Fellow with CityU HK, in 2014. His main research interests include evolutionary computation, multiobjective optimization, and the development of algorithms with practical applicability. He was a recipient of the Operational Research Society Ph.D. Runner-Up Prize for the Best Ph.D. Dissertation, in 2014, and the Funds for Distinguished Young Scientists from the Natural Science Foundation of Hunan, in 2016.

MENGJUN MING was born in 1993. She is currently pursuing the Ph.D. degree with the National University of Defense Technology. Her research interests include evolutionary computation and the optimization of energy systems.